ChemistrySelect

ChemistrySelect
Chemistry Europe
European Chemical Societies Publishing

RESEARCH ARTICLE OPEN ACCESS

One-Step Fabricated Green Tubular Ceramic Membrane for Chromium (VI) Removal With High Permeability and Low Production Cost

Mhamed A. Aburawi[1,2] | Almahdi A. Alhwaige[3] | Afef Attia[1] | Hajer Aloulou[1,4] | Zahia Tigrine[5] | Seif El Islam Lebouachera[6] | Raja Ben Amar[1]

[1]Advanced Technologies for Environment and Smart Cities, Faculty of Science of Sfax, University of Sfax, Sfax, Tunisia | [2]Department of Chemistry, Faculty of Education, Alasmarya Islamic University, Zliten, Libya | [3]Department of Chemical Engineering, University of Tripoli, Tripoli, Libya | [4]Department of Chemistry, Preparatory Institute for Engineering Studies of Gabes, University of Gabes, Gabes, Tunisia | [5]Unité de Développement des Equipements Solaires (UDES), Centre de Développement des Energies Renouvelables (CDER), Bou-Ismail, Algeria | [6]Institut Des Sciences Analytiques Et De Physico-Chimie Pour L'Environnement Et Les Matériaux, IPREM, UMR 5254, Technopôle Hélioparc, CNRS Université de Pau et Des Pays de L'Adour, Pau, France

Correspondence: Raja Ben Amar (raja.benamar@fss.usf.tn)

Received: 10 November 2025 | **Revised:** 1 May 2026 | **Accepted:** 10 June 2026

Keywords: barley husk | ceramic membranes | Cr (VI) removal | Libyan kaolin | sand

ABSTRACT

Large volumes of wastewater are released into the environment without proper treatment. Water pollution is linked to over 80% of diseases and deaths each year. Contamination by heavy metal ions arises from both natural sources and human activities. Among these, hexavalent chromium (Cr(VI)) is one of the most toxic metals, causing severe toxicity and bioaccumulation. The development of effective water treatment technologies is therefore critical to mitigate these harmful effects. Membrane filtration has emerged as a promising approach due to its simplicity, cost-effectiveness, and high efficiency. In this study, green tubular ceramic membranes (GTCMs) were fabricated from Libyan kaolin clay (LKC), natural sand, and barley husk (BH) for the removal of Cr(VI). The optimized membrane ($C_{77}S_{20}BH_3$-T_{950}) was characterized by Fourier transform infrared spectroscopy, atomic force microscopy (AFM), and scanning electron microscopy (SEM). Membrane performance was investigated by determining membrane permeability and chromium retention rate. This membrane exhibited an average pore size of 56.4 nm, a porosity of 34.28%, and a high water permeability of approximately ~476 $L.h^{-1}.m^{-2}.bar^{-1}$. The membrane's performance for Cr(VI) removal was evaluated, achieving a maximum removal efficiency of 87.24% at an initial concentration of 2.5 ppm and pH 2, highlighting its strong potential for heavy metal ion removal from aqueous solutions.

1 | Introduction

Membrane separation has emerged as a prominent technique for water purification due to its straightforward design, compact size, absence of chemical additives, low energy requirements, and high efficiency [1–4]. Among the different types of membranes, ceramic membranes have shown exceptional performance in removing heavy metals such as Pb(II), Cu(II), and Ni(II) [5, 6]. Consequently, the application of membrane technologies for the removal of heavy metals has expanded significantly in recent years [1, 2, 5–9].

Water pollution caused by heavy metal ions, originating from both natural sources and human activities, is highly hazardous and accounts for over 80% of waterborne diseases and related deaths [9–12]. Among these metals, hexavalent chromium ions

(Cr(VI)) are particularly toxic, posing serious threats to human health, including carcinogenic effects and damage to the eyes, skin, kidneys, and liver, due to their high toxicity and potential for bioaccumulation [2, 7]. Cr(VI) ions can be released through various industrial processes, including mining, metal and alloy production, electroplating, dye manufacturing, plastics, paints, paper production, battery industries, as well as hospital and municipal effluents [8, 12].

According to the World Health Organization (WHO), the maximum allowable concentration of total chromium in drinking water is 0.05 mg/L [9, 13]. For hexavalent chromium specifically, some global guidelines recommend a stricter limit of 0.05 $mg.L^{-1}$ due to its significant environmental issues and carcinogenic potential [12, 14]. In Tunisia, national standards for wastewater discharge (NT 106.002) permit a maximum chromium concentration of 0.5 $mg.L^{-1}$ before discharge into the environment [15]. Although chromium naturally occurs as the less toxic Cr(III) ions, industrial processes can oxidize it to the far more hazardous Cr(VI) form. Cr(VI) is approximately 100 times more toxic than Cr(III) due to its high solubility, mobility, and reactivity [9, 10]. Industrial effluents frequently contain chromium concentrations ranging from 0.5 to 270 $mg.L^{-1}$, significantly exceeding the WHO guideline for potable water [11, 12].

This considerable discrepancy has driven extensive research into the development of selective membranes for chromium ion removal. In particular, ceramic membranes derived from metal oxides and natural inorganic materials, such as clay, have shown great promise. These membranes enable ultrafiltration (UF) systems to selectively remove heavy metals due to their unique properties, including tunable pore size and structure, high porosity and adsorption capacity, ease of functionalization and integration into base materials, controllable hydrophilicity, chemical and thermal stability, and reusability [2, 8, 9].

Ceramic membranes have gained increasing attention in separation processes owing to their outstanding features such as thermal stability, chemical resistance, high mechanical strength, ease of cleaning, and long operational lifespan [3, 16]. Nevertheless, their large-scale application remains constrained by high production costs, mainly arising from the use of expensive raw materials such as alumina (Al_2O_3), zirconia (ZrO_2), and titania (TiO_2) and the energy-demanding sintering process, typically conducted at 1300°C–1500°C [17, 18]. Consequently, current research efforts are directed toward developing cost-effective ceramic membranes from alternative raw materials, sintered at lower temperatures (<1000°C) [9, 19].

Naturally abundant clays, including kaolin, bentonite, and montmorillonite, have been widely explored as cost-effective raw materials [4, 19]. Among them, kaolin clay is particularly valued for its excellent hydrophilicity and mechanical strength. However, a major challenge in clay-based membranes is the significant shrinkage that occurs during sintering, which can reduce the permeate flux [20]. To address this issue and improve porosity, various affordable pore-forming agents have been incorporated into the membrane matrix. Agricultural residues such as rice husks, coconut husks, and cow bones have been shown to be highly effective for this application [8, 16–24]. In particular, grain husks have been found to produce distinctive microstructures, resulting in high permeability and superior separation performance [24]. While ceramic membranes have been successfully manufactured using clays from Tunisia [1, 9, 17, 25–27], Algeria [7, 28], and Morocco [4, 29–31] to the best of our knowledge, the potential of Libyan kaolin clay (LKC) for this purpose has yet to be thoroughly investigated as no prior reports exist on its use for ceramic membrane fabrication in water treatment applications.

Nanofiltration (NF) is widely used for the removal of salts and heavy metals; however, it is often considered energy-intensive, and NF membranes typically exhibit low water permeability [32–35]. As a result, extensive research has focused on modifying UF membranes through coating, grafting, blending, and other approaches to develop functionalized UF membranes capable of removing dissolved pollutants [9, 35, 36]. For example, adsorptive membranes, which combine high permeability with a strong capacity for heavy-metal ion removal, are gaining increasing attention [37, 38]. These membranes can operate at low pressure, offering a promising alternative that avoids the need for heavy infrastructure associated with high-pressure processes such as reverse osmosis and NF.

This study introduces a novel strategy for developing green tubular ceramic membranes (GTCMs) utilizing low-cost LKC and barley husk (BH) as a bio-based pore-forming additive, applied here for the first time. The originality of this work lies in optimizing the physicochemical properties of these locally sourced clay-derived membranes to achieve effective removal of Cr(VI). The proposed approach aims to combine economic feasibility, environmental sustainability, and enhanced selectivity. A thorough assessment is conducted covering membrane fabrication, structural characterization, and the performance of the GTCMs in treating aqueous solutions contaminated with Cr(VI).

2 | Experimental Procedure

2.1 | Raw Materials

LKC (LKC, particle size ≈100 μm) and BHs (particle size ≈350 μm) were collected from Zliten, northern Libya. The LKC was used unprocessed, without leaching or purification. While the clay contains minor amounts of other metal oxides (Fe_2O_3, CaO, and MgO), these impurities were intentionally retained: they serve as fluxing agents to lower the sintering temperature and provide additional surface functional groups that may assist heavy metal adsorption. This approach aligns directly with the study's goal of producing a low-cost, green, and sustainable ceramic membrane. Natural silica sand powder (particle size ≈100 μm) was sourced from Gharyan, Libya. Potassium dichromate ($K_2Cr_2O_7$), sodium hydroxide (NaOH), and sulfuric acid (H_2SO_4) were obtained from Merck Chemical (Germany), all of analytical grade. Distilled water (pH 7.4, electrical conductivity 0.8 μS/cm) was used for the preparation of all solutions.

2.2 | Fabrication of Green Ceramic Membranes

The GTCMs based on LKC were fabricated through sequential steps including batching, mixing, extrusion, drying, and

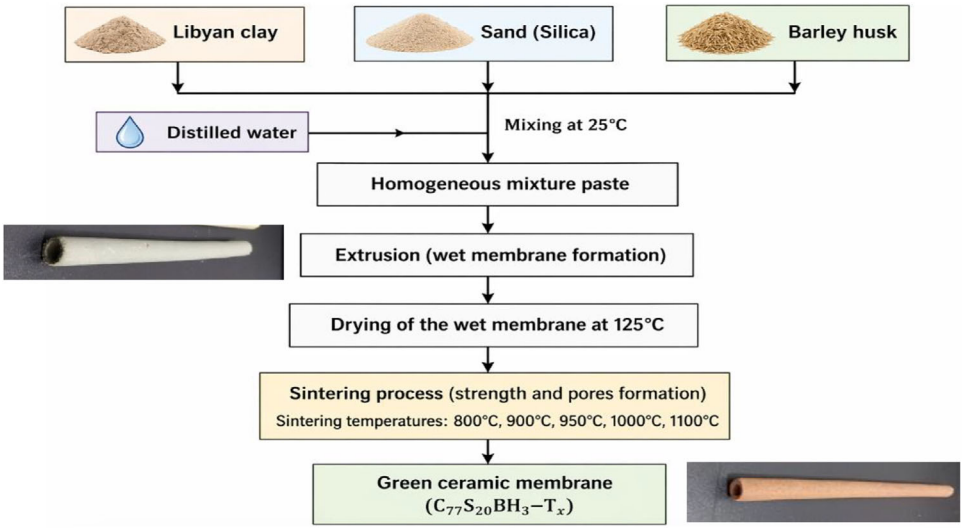

FIGURE 1 | Preparation steps of the GTCMs by the extrusion method.

TABLE 1 | The abbreviations and compositions of the GTCMs.

Membrane code	Content (wt%)		
	Libyan kaolin Clay (C)	Natural Sand (S)	Barley Husk (BH)
$C_{80}S_{20}BH_0$-T_N	80	20	00
$C_{77}S_{20}BH_3$-T_N	77	20	03

Note: The subscripted letter "N" represents the sintering temperatures of 150 °C, 800 °C, 850 °C, 900 °C, 950 °C, 1000 °C, and 1050°C.

sintering, as illustrated in Figure 1. In the first stage, a clay-based paste was prepared by blending LKC, natural sand, and BH using a mechanical mixer at room temperature, with the gradual addition of 20 mL of distilled water. Natural sand was incorporated to enhance the mechanical strength and thermal stability of the ceramic membranes [39, 40], while BH served as a bio-based pore-forming agent. The selection of the specific compositions presented in Table 1 was guided by preliminary optimization experiments and established principles in low-cost ceramic membrane fabrication. The base ratio of 80 wt% LKC to 20 wt% natural sand was chosen because the clay content ensures sufficient plasticity for extrusion and provides the aluminosilicate phase necessary for mechanical strength and surface functionality, while the 20 wt% sand acts as an inert filler to reduce shrinkage during sintering and improve thermal stability [17, 39, 40]. The 3 wt% BH content was determined through an independent optimization study (data not shown) in which BH was varied from 0 to 10 wt%. It was found that 3 wt% BH offered the optimal balance: increasing porosity and permeability without excessively compromising mechanical integrity. Higher BH contents (≥5 wt%) led to excessive porosity (>45%) and a significant drop in mechanical strength (below 15 MPa), making the membranes unsuitable for practical crossflow filtration applications. This trend is consistent with literature reports on agricultural waste-derived pore-forming agents [21, 29, 41]. After 10 min of continuous mixing, a thick and homogeneous paste was obtained, which was then transferred to a plastic plate and aged for 24 h [10, 17].

In the second stage, the aged paste was molded into rectangular-flat and tubular membrane modules using a manual hydraulic press [42]. The rectangular membranes (4.5 cm × 2 cm × 0.5 cm) were prepared for mechanical and contact angle characterization, while tubular membranes (16 cm in length, with inner and outer diameters of 0.5 cm and 1 cm, respectively) were fabricated for further testing.

Finally, the dried membranes were sintered at different temperatures: 800 °C, 850 °C, 900 °C, 950 °C, 1000 °C, and 1050°C. The produced ceramic tubular membranes were marked as $C_XS_YBH_Z$-T_N, where *X* represents the content of added LKC (C), *Y* represents the availability composition of natural sand (S), and *Z* refers to the wt% of BH in the membrane. The letter *N* represents the thermal treatment temperature (*T*) of the dried membrane (in °C). The abbreviations and contents of the starting materials in the fabricated GTCMs are summarized in Table 1.

2.3 | Characterizations

The composition of the LKC and natural sand powders was investigated. Elemental analysis of the clay was performed using an ARL PERFORM'X X-Ray Fluorescence (XRF) spectrometer (Thermo Fisher Scientific) at the laboratory of Elmergib Cement Factory, Al-Khoms, Libya.

The crystallinity of both the kaolin powder and the $C_{77}S_{20}BH_3$-T_{950} membrane was examined using a powder x-ray diffractometer (PANalytical, The Netherlands, Model: PW3040/60 X'pert PRO) equipped with a 3 kW Cu x-ray tube. Measurements were conducted using Cu Kα radiation (λ = 1.5406 Å) over a 2θ range of 5° to 90°, with a scanning rate of 1° per min.

Scanning electron microscope (SEM) technique was employed to study the morphology of the optimized membrane. SEM images of the derived membranes were obtained using a model, jsm 5610 LV Acce .volt, from 5 to 30 kV.

The surface wettability of the produced GTCMs was assessed using static contact angle measurements with a Ramé–Hart Instrument Co. model 200-F4 goniometer. A 3 µL droplet of pure water was deposited onto the membrane surface using a syringe equipped with a fine needle. The contact angle of the sessile droplet on the membrane was recorded under ambient conditions. To ensure reliable results, measurements were taken at multiple locations across the membrane surface. The reported contact angle represents the average of these measurements.

The topography, height, and roughness of the $C_{77}S_{20}BH_3$-T_{950} membrane were examined using atomic force microscopy (AFM). The AFM imaging was performed with an NCLR rectangular-shaped silicon cantilever with a resonant frequency of 130 kHz. at room temperature.

The apparent bulk density (ρ_b) of $C_{80}S_{20}BH_0$ and $C_{77}S_{20}BH_3$ ceramic membranes was obtained from the membrane mass and its volume as described in Equation (1) [43].

$$\rho_b = \frac{m}{V} \tag{1}$$

where m is the membrane mass (g), and V is the membrane volume (cm).

The porosity of the GTCMs was determined using the gravimetric method. Each membrane sample was first weighed in its dry state. The samples were then immersed in distilled water for 24 h and subsequently weighed in the wet state after gently wiping the surface with dry tissue paper. Membrane porosity was calculated according to Equation (2b) [3, 44].

$$\varepsilon\,\% = \left(\frac{m_{\mathrm{w}} - m_{\mathrm{d}}}{\rho A h}\right) \times 100 \tag{2a}$$

$$\varepsilon\,\% = \left(\frac{4\,(m_{\mathrm{w}} - m_{\mathrm{d}})}{\pi * \rho\,(D_o^2 - D_i^2)\,L}\right) \times 100 \tag{2b}$$

where ε is the porosity of the membrane (%), m_{w} is the wet mass of the membrane and m_{d} is the dry mass of the membrane (kg), ρ is the water density (998 kg.m^{-3}), A is the membrane surface area (m^2), h is the membrane thickness (m), D_o and D_i are the outer and inside diameters of the tubular membrane, respectively, and L is the membrane length (m). To avoid experimental error, five values were taken, averaged, and reported.

Pore size is a critical factor influencing the separation efficiency of membranes. Accordingly, the mean pore diameter of the prepared ceramic membranes was estimated using Equation (3) [3, 4].

$$d_p = 2\left(\frac{8\mu h L_p}{\varepsilon}\right)^{0.5} \tag{3}$$

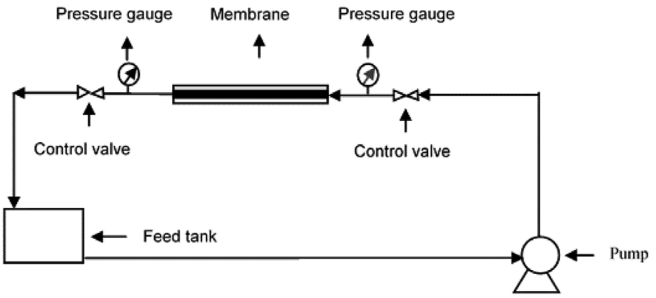

FIGURE 2 | Schematic diagram of the used membrane unit.

where d_p is the mean pore diameter (m), ε is the membrane porosity, μ is the water viscosity (8.9×10^{-4} Pa.s), h is the membrane thickness (m), and L_p is the permeability (m^3.s^{-1}.m^{-2}.Pa^{-1}).

The shrinkage of GTCMs was determined according to the change in the membrane diameter before and after the sintering process. The shrinkage % was determined as given in Equation (4) [45].

$$Shrinkage\,\% = \left(\frac{D_o - D}{D_o}\right) \times 100 \tag{4}$$

where D_o and D are the initial membrane diameter and its diameters after thermal treatment (mm), respectively.

The effect of sintering temperatures on the mechanical strength of the $C_{77}S_{20}BH_3$-T_{950} was also evaluated. The mechanical strength of the ceramic membrane was measured using the three-point bending strength method using a laboratory-scale apparatus (Lloyd Instrument, Bognor Regis, UK). A sample with dimensions of 45 mm × 20 mm × 5 mm was set on two supports with a gap of 30 mm between them. After a force F was applied to the three-point bending on the sample, the highest breaking force was recorded in Newton. The experiments were evaluated at various thermal temperatures to study the effect of sintering temperature on the strength of the membrane [45]. The chemical stability of the GTCMs in acidic and basic media was evaluated. Membrane samples were immersed in aqueous HCl (pH 1.5) or NaOH (pH 13) solutions for 7 days, and their chemical stability was assessed based on the resulting weight loss [42, 46]. The percentage of weight loss was calculated according to Equation (5).

$$Weight\ loss\,\% = \left(\frac{\mathrm{W_o} - \mathrm{W}}{\mathrm{W_o}}\right) \times 100 \tag{5}$$

Where W_o and W are the sample initial weight and the sample weight after a time interval of soaking in the aqueous solution (mg), respectively.

2.4 | Measurement of the Membrane Permeability

The water flux and permeability of $C_{80}S_{20}BH_0$ and $C_{77}S_{20}BH_3$ were measured using a continuous flow membrane system (see Figure 2) with an effective surface area of 52 cm^2. Membranes were pre-soaked in distilled water for 24 h to achieve stable permeate flux, following Bousbih et al. [17]. Experiments were conducted at 25°C under pressures ranging from 0.5 to 3.0 bar.

Permeate volume (V_w) was collected over a known time interval (Δt), and the pure water flux (J_w) was calculated using Equation (6). Water permeability was determined by measuring the permeate flux at different pressures at room temperature. The permeability of each membrane was calculated from the slope of the permeate flux versus pressure plot, as described in Equation (7) [25, 26, 42, 44].

$$J_w = \left(\frac{V_w}{A \times \Delta t} \right) \tag{6}$$

$$J_w = L_p \times \Delta P \tag{7}$$

where J_w is the permeate flux ($L.h^{-1}.m^{-2}$), A is the membrane effective surface area, which was measured using the inner diameter (m^2), V_w is the water permeate volume (L), and Δt is the interval of the permeate time (h). L_p is the membrane permeability ($L.h^{-1}.m^{-2}.bar^{-1}$), and ΔP is the pressure drop between the two sides of the membrane (bar).

2.5 | Evaluation of the Ceramic Membranes for Cr(VI) Rejection

The prepared $C_{77}S_{20}BH_3$-T_{950} membrane was employed for the treatment of Cr(VI) contaminated water under various operating conditions. A stock solution of 1000 ppm $K_2Cr_2O_7$ was first prepared using distilled water and subsequently diluted to 2.5, 5, and 10 ppm for the Cr(VI) removal experiments using the fabricated ceramic membranes. Prior to testing, the membrane was pre-wetted with distilled water to ensure proper evaluation of Cr(VI) rejection from the aqueous feed solution [26].

In each experiment, 4 L of the $K_2Cr_2O_7$ aqueous solution was passed through the membrane system at a controlled flow rate for 4 h. The operating pressure was regulated using an adjustable valve positioned between the pump and the membrane. During the process, permeate samples were collected at regular time intervals. Cr(VI) concentrations in both the feed and permeate were determined using atomic absorption spectroscopy (AAS) [1]. The Cr(VI) rejection efficiency ($R\%$) was calculated according to Equation (8) [17, 25, 47].

$$R\,\% = \left(1 - \frac{C_p}{C_f} \right) \times 100 \tag{8}$$

where $R\%$ is the rejection efficiency of the Cr(VI), C_f, and C_p are the feed and permeate concentrations of the Cr(VI) in $mg.L^{-1}$, respectively.

All experiments were performed in triplicate to ensure the reproducibility and reliability of the results. The obtained data are presented as mean values ± standard deviation.

The membrane regeneration was determined by water rinsing in the first stage, followed by a chemical treatment with an alternative circulation of 2% solutions of NaOH at 80°C and HNO_3 at 60°C for 30 min. Finally, the membrane was rinsed with distilled water until a neutral pH was checked. The effectiveness of the cleaning protocol was confirmed by measuring the water permeability after the cleaning cycle, which must be almost equal to that of the new membrane.

The fouling characteristic of the membranes was evaluated by calculating the flux recovery ratio (FRR) using Equation (9).

$$FRR = \frac{J_{WA}}{J_W} \times 100 \tag{9}$$

where J_W is the water flux of the new membrane, and J_{WA} is the water permeate flux of the membrane measured after rinsing the used membrane with distilled water.

3 | Results and Discussion

3.1 | Mineralogical Compositions of Used Libyan Natural Clay

The chemical composition of the used LKC was investigated, and the results are illustrated in Table 2. The major chemical components in the natural LKC are silica (SiO_2: 62.93%) and alumina (Al_2O_3: 14.44%). In addition, it consists of a lower proportion (~ 6.36 wt%) of iron(III) oxide. Therefore, the light brown color of the sintered membrane was ascribed to the existence of iron (III) oxide. The change in color of sintered ceramic membranes to brown color was previously observed [26, 48]. Furthermore, other oxides such as calcium, magnesium, potassium, and sulfur oxides were also present in very low amounts. For the sand, the major chemical component is silica (SiO_2: 98.25%). These findings are consistent with the early reported elemental analysis of other clay types [42, 48].

3.2 | Characterizations of the Green Ceramic Membranes as Function of BH Incorporation and Sintering Temperature

3.2.1 | Shrinkage and Porosity

The shrinkage in the GTCMs after the sintering process was evaluated. In Figure 3, the dashed lines demonstrate the effects of sintering temperatures on the membranes' shrinkage during thermally treating of the membranes at100 °C, 500 °C, 800 °C, 900 °C, 950 °C, 1000 °C, and 1050°C. The results demonstrated that both the GTCMs have similar shrinkage behaviors. Therefore, the shrinkage values of the membranes were gradually increased with an increase in the sintering temperature. The shrinkage in the $C_{80}S_{20}BH_0$-T_{950} and $C_{77}S_{20}BH_3$-T_{950}ceramic membranes that sintered at a temperature of 950°C were found to be 6% and 15%, respectively. The decrease in the shrinkage rate after sintering temperatures higher than ~950°C was observed, which is ascribed to the process of densification at temperatures greater than 950°C [45]. In addition, the shrinkage value in the membrane that contains the BH ($C_{77}S_{20}BH_3$) was higher than the BH-free membrane ($C_{80}S_{20}BH_0$) due to the effect of membrane porosity. These observations are in good agreement with previously reported studies for ceramic membrane shrinkage [19].

In addition, the effect of the presence of BH in the GTCMs membranes' porosity has been investigated (see Figure 3). The

TABLE 2 | The chemical composition of the Libyan kaolin clay and the natural sand.

	Chemical composition (wt%)										
Material	**CaO**	**SiO_2**	**Fe_2O_3**	**K_2O**	**MgO**	**MnO**	**Na_2O**	**P_2O_5**	**SO_3**	**TiO_2**	**Al_2O_3**
Libyan kaolin clay	6.41	62.93	6.36	0.72	1.87	0.032	0.036	0.177	1.640	0.810	14.44
Natural sand	—	98.25	0.15	—	0.04	—	—	—	—	0.13	1.16

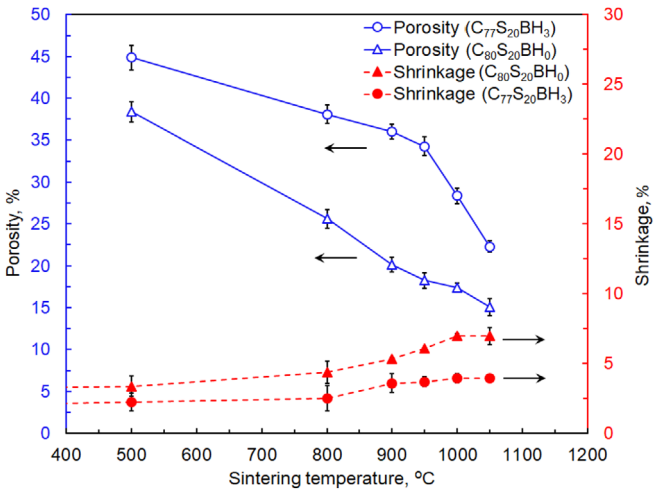

FIGURE 3 | Effect of sintering temperatures on the GTCMs: (i) The porosity (solid line) and (ii) the shrinkage in the membrane volume (dashed line).

porosity of the GTCMs has been increased after modifying the clay/natural sand membrane with BH, which is ascribed to the creation of new pores after pyrolysis of available BH. Based on the literature, Njuhou et al. [41] reported that rice husk leads to an increase in porosity, permeability, and hydraulic diameter of kaolin-based ceramic membranes due to decomposition of organics during membranes' thermal treatment. Furthermore, the influence of the sintering temperature of the membrane porosity has been also studied. The results indicated that the porosity has an inverse relationship with thermal treatment. For example, the porosity of $C_{77}S_{20}BH_3$-$T_{950}$was decreased from 44.85% to 34.28% with an increase in the sintering temperature from 500°C to 950°C. Additionally, a linear reduction in the porosities of the $C_{80}S_{20}BH_0$ was observed; however, the drop in the porosities $C_{77}S_{20}BH_3$ has a nonlinear relationship with sintering temperature. The significant reduction in the porosity of GTCMs after sintering at 950°C is attributed to the shrinkage in the membrane volume, which may relate to self-compression (see dashed lines in Figure 3). Similar findings were observed for *Rosmarinus officinalis L*-modified kaolin ceramic membrane [29].

3.2.2 | Chemical Stability

Figure 4 displays the effect of sintering temperature on the weight loss of the soaked sintered $C_{80}S_{20}BH_0$ and $C_{77}S_{20}BH_3$ green ceramic membranes in HCl and NaOH solutions. The findings demonstrated that the GTCMs had appropriate weight loss (< 1.2%) and high chemical stability in both acidic and basic media. Previously, it was reported that clay-based ceramic membranes showed poor stability in acid solution, which is ascribed to the presence of dickite and nacrite that are relatively sensitive to acidic environments [42]. In the case of $C_{77}S_{20}BH_3$, the samples with different sintering temperatures indicate < 0.3% weight loss in basic medium. Therefore, BH reduced the chemical degradation of the $C_{80}S_{20}BH_0$ ceramic membrane. Consequently, the $C_{77}S_{20}BH_3$ membrane demonstrated greater structural stability than the $C_{80}S_{20}BH_0$ membrane, a performance that was further improved by lowering the sintering temperature. Overall, the results confirmed that the GTCMs have excellent corrosion resistance in both acidic and basic media [20].

Therefore, according to the shrinkage, porosity, as well as the chemical resistances of GTCMs membranes, 950°C can be considered as the optimal sintering temperature.

3.3 | Characterization of the Green Ceramic Membranes as Function of BH Incorporation

3.3.1 | Permeate Flux and Water Permeability of the GTCMs Membranes

Flux and permeability of distilled water are considered important properties for the development of new membranes [17, 49]. Figure 5 shows the distilled water flux of resulting ceramic membranes derived from Libyan clay with and without BH after being thermally treated at 950°C ($C_{80}S_{20}BH_0$-T_{950} and $C_{77}S_{20}BH_3$-T_{950}) at ambient temperature for 100 min. At 3 bar, the $C_{80}S_{20}BH_0$-T_{950} and $C_{77}S_{20}BH_3$-T_{950} ceramic membranes showed water permeability of ~580.2 and ~1318.7 $L.h^{-1}.m^{-2}$, respectively. In addition, the ceramic membranes demonstrated stable fluxes after 20 min of filtration, and then a slight decrease was observed (see Figure 5a). After 60 min of processing time, the permeate flux decreased slightly by ~7.51% and ~1.89% for $C_{80}S_{20}BH_0$-T_{950} and $C_{77}S_{20}BH_3$-T_{950} ceramic membranes, respectively. This behavior of permeate flux of pure water is consistent with previously reported investigations [17, 19, 30, 45]. Furthermore, the results indicated that $C_{77}S_{20}BH_3$-T_{950} has higher flux than the $C_{80}S_{20}BH_0$-T_{950}, which is ascribed to the increase in the membrane porosity due to the addition of BH [21, 29, 41].

On the other hand, applied pressure is considered one of the important parameters that effects on water fluxes of membrane systems [3, 30]. Figure 5b illustrates the relationship between the permeate flux of distilled water and the applied pressure for $C_{80}S_{20}BH_0$-T_{950} and $C_{77}S_{20}BH_3$-T_{950} ceramic membranes. Both membranes exhibit a similar behavior, with permeate flux increasing proportionally with applied pressure, a typical characteristic of membrane fluxes [30, 50]. High permeate flux

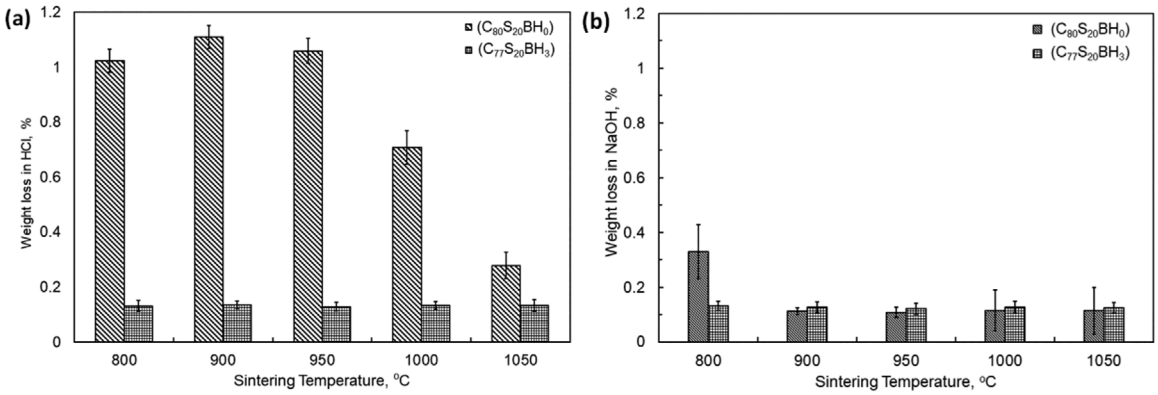

FIGURE 4 | Variation of weight loss of GTCMs membrane with sintering temperatures in different media: (a) in HCl (pH = 1.5) and (b) in NaOH (pH = 13).

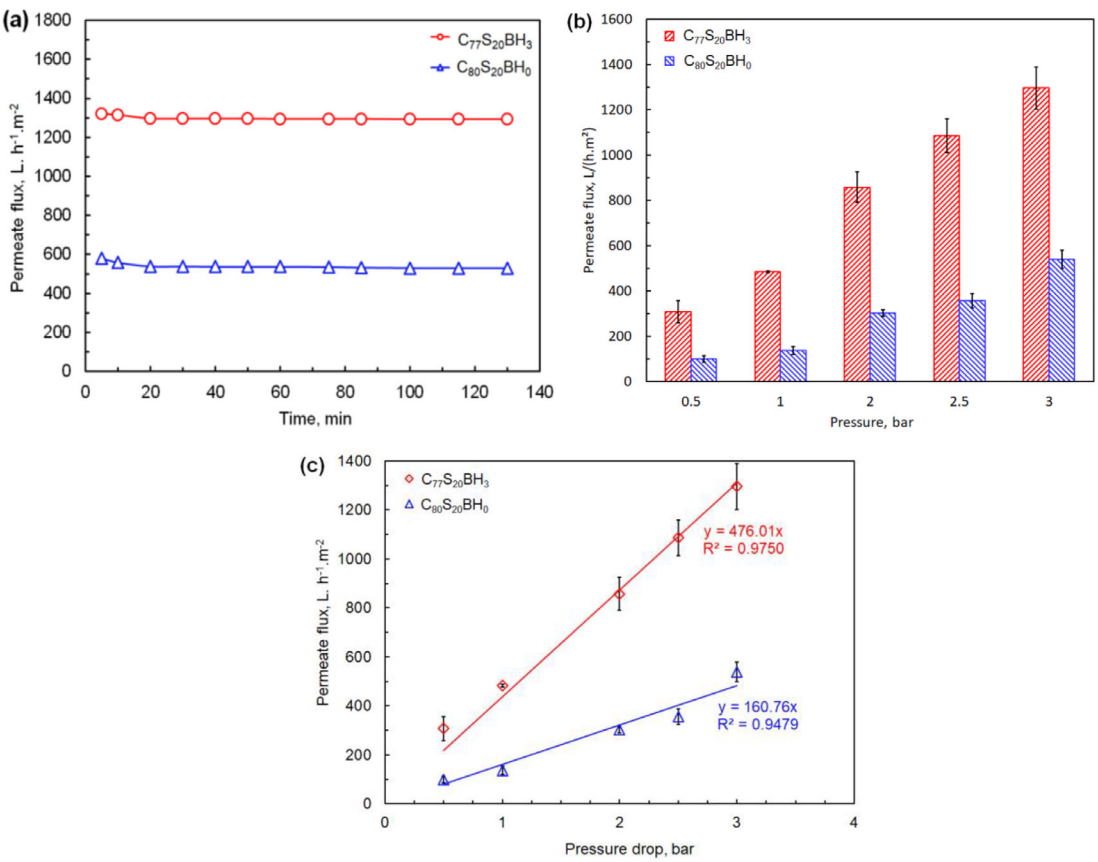

FIGURE 5 | Determination of the membrane water permeability performance with both membranes: (a) Permeate flux at a pressure of 3 bar and room temperature. (b) Effect of pressure on water permeate flux after 30 min. (c) Determination of the variation of Permeate flux versus transmembrane pressure.

is essential for achieving efficient water production in various applications, including seawater desalination and wastewater treatment [18, 51–53].

The permeability values of the GTCMs ceramic membranes were also evaluated. Figure 5c shows that the permeate flux has a linear-proportional relationship with the applied pressure for the studied ceramic membranes that were sintered at 950°C ($C_{80}S_{20}BH_0$-T_{950} and $C_{77}S_{20}BH_3$-T_{950}) [20, 24]. The results indicated that the average permeability values of $C_{80}S_{20}BH_0$-T_{950} and $C_{77}S_{20}BH_3$-T_{950}membranes were found to be 160.75 and 476.01 $L.h^{-1}.m^{-2}.bar^{-1}$, respectively. Therefore, the permeability values of both membranes were in order of $L_{p,}C_{77}S_{20}BH_{3}$-$T_{950} \geq L_{p,}C_{80}S_{20}BH_{0}$-$T_{950}$.

TABLE 3 | Determination of densities, porosities, and water permeability for the GTCMs after sintering at 950°C.

Membrane code	Density ($kg.m^{-3}$)	Porosity (%)	Pore size (μm)	Permeability ($L.h^{-1}.m^{-2}.bar^{-1}$)
$C_{80}S_{20}BH_0$-T_{950}	1804	18.25	4.39×10^{-2}	160.75
$C_{77}S_{20}BH_3$-T_{950}	1719	34.28	5.64×10^{-2}	476.01

TABLE 4 | Comparative study with properties of other various low-cost natural organic materials-derived clay-based ceramic membranes reported in the literature.

Raw material	Sintering Temp. (∘C)	Pore size (μm)	Porosity (%)	Mechanical strength (MPa)	Permeability ($L.h^{-1}.m^{-2}.bar^{-1}$)	Ref.
Libyan kaolin clay/sand/BH[a]	950	0.056	34.28	33.86	∼476	This study
Tunisian kaolin/sand	900	0.017	44.72	15.14	491	[1]
Tunisian kaolin	1000	0.035	26.00	13.00	21.2	[17]
Tunisian sand	1100	10.36	40.00	N/A[b]	N/A	[27]
Moroccan Kaolin/*RO*[c]	1100	01.05	30.15	57.16	N/A	[29]
Moroccan red clay/banana	1100	05.50	40.00	19.20	550	[31]
Cameroon kaolin/rice husk	1050	02.60	30.0	08.00	675	[41]
Silica/rice husk	1200	0.55–2.3	43.1	71.20	N/A	[54]
Metakaolin-Corn cob ash	1200	03.26	62.03	41.61	N/A	[56]

[a]BH: Barley husk.
[b]N/A: Not applicable.
[c]*RO*: *Rosmarinus officinals*.

In summary, the water flow through the membrane remained constant for 2 h of operation, which encourages the use of the $C_{77}S_{20}BH_3$-T_{950} ceramic membrane for water separation streams [42, 50].

3.3.2 | Density and Pore Size

Table 3 illustrates the density of the obtained ceramic membranes at 950°C. The results indicated that the density of $C_{77}S_{20}BH_3$-T_{950} membrane was lower than BH-free membrane ($C_{80}S_{20}BH_0$-T_{950}). The densities $C_{80}S_{20}BH_0$-T_{950} and $C_{77}S_{20}BH_3$-T_{950} were found to be 1804 and 1719 $kg.m^{-3}$, respectively. The reduction in the density of $C_{77}S_{20}BH_3$-T_{950} is attributed to the increase in porosity due to the availability of natural sand and BH. Previously, it was found that agricultural waste-based materials play a role in improving the properties of clay-derived ceramic membranes [20, 21, 29, 41, 54, 55].

The estimated pore sizes of the GTCMs membranes were found to be 4.39×10^{-2} and 5.64×10^{-2} μm for $C_{80}S_{20}BH_0$-T_{950} and $C_{77}S_{20}BH_3$-T_{950}, respectively. It is clear that the addition of the BH in the membrane composition increases the pore size. From Table 3, it was found that the incorporation of the BH improved the membrane properties so the $C_{77}S_{20}BH_3$-T_{950} membrane was selected as the optimized membrane for this study.

As shown in Table 4, the $C_{77}S_{20}BH_3$-T_{950} membrane exhibits performance comparable to other clay-based membranes reported in the literature. For instance, a kaolin/rice-husk membrane with approximately 30% porosity achieved a permeability of 675 $L.h^{-1}.m^{-2}.bar^{-1}$ [41]. In comparison, the $C_{77}S_{20}BH_3$-T_{950} membrane, featuring 34.28% porosity, an average pore size of 5.64×10^{-2} μm, and a permeability of ∼476 $L.h^{-1}.m^{-2}.bar^{-1}$ demonstrates competitive transport performance. Additionally, it benefits from significantly higher mechanical strength relative to many other high-permeability clay-based membranes, highlighting its robustness and application potential.

3.4 | Characterizations of the Optimized Membrane ($C_{77}S_{20}BH_3$-T_{950})

3.4.1 | Morphological and Microstructure Analysis

Figure 6 presents SEM images of the $C_{77}S_{20}BH_3$ ceramic membrane before and after the sintering process. Figure 6a shows a cross-sectional image of the membrane without thermal treatment, revealing a non-porous surface with BH embedded within the membrane matrix. After sintering, the porosity of the ceramic membrane is significantly enhanced. Figures 7b and 6c illustrate the morphology of the $C_{77}S_{20}BH_3$-T_{950} membrane sintered at 950°C. SEM analysis indicates that the clay particles on the membrane surface agglomerated during sintering, resulting in a rough surface (Figure 6b). This rough morphology contributes to the development of a porous structure, improving membrane permeability [57]. As shown in Figure 6b, pores are clearly visible on the membrane surface, and the membrane is free of defects. Moreover, the distribution of pores across the membrane surface is heterogeneous, indicating a varied morphology.

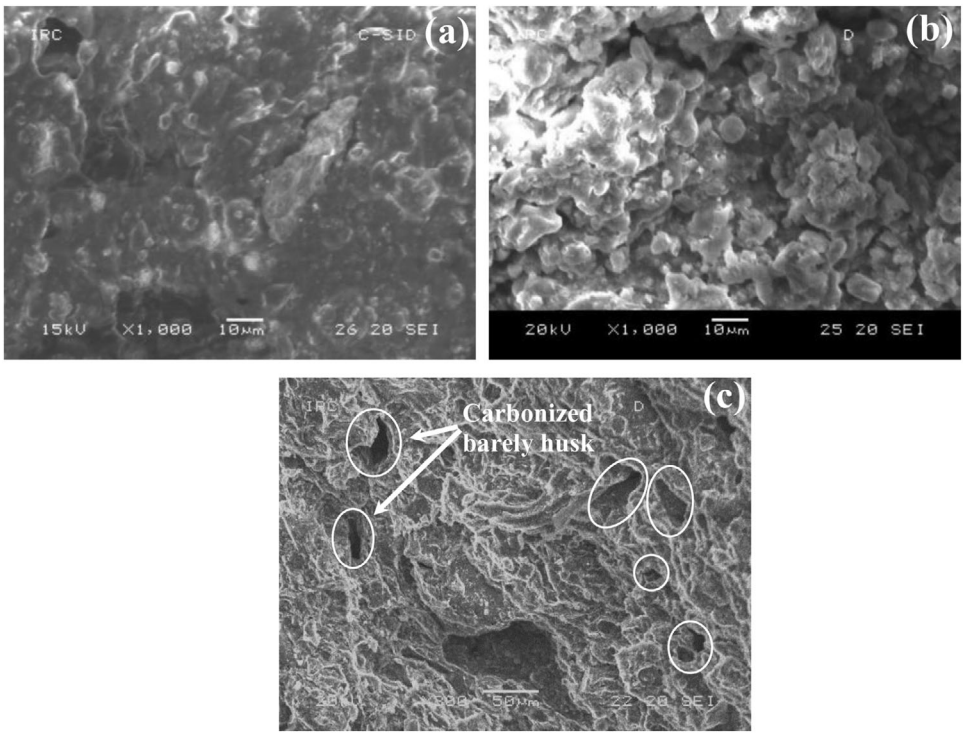

FIGURE 6 | SEM micrographs of the $C_{77}S_{20}BH_3$ ceramic membrane: (a) surface section of $C_{77}S_{20}BH_3$ before sintering; (b) surface and (c) cross section of $C_{77}S_{20}BH_3$-T_{950}.

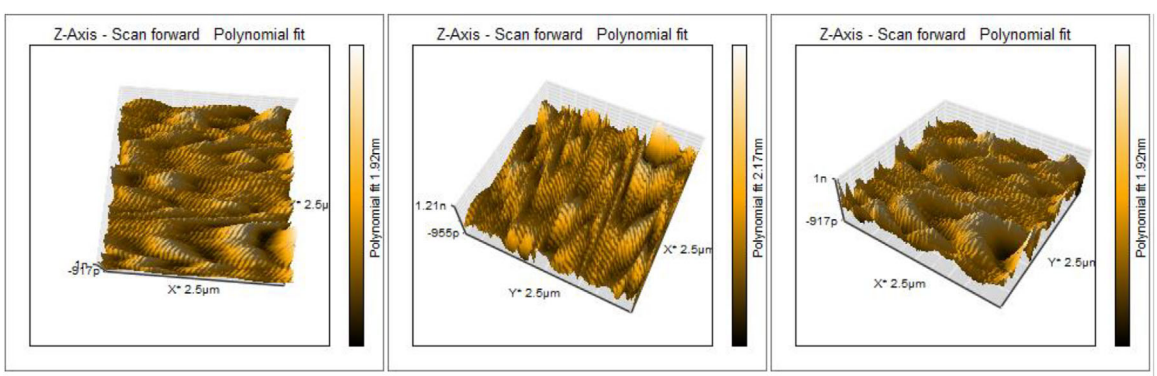

FIGURE 7 | Atomic force micrographs (AFM) of $C_{77}S_{20}BH_3$-T_{950} ceramic membrane.

As shown in Figure 6c, the cross-sectional micrographs reveal that the membrane exhibits a porous structure. The effect of incorporating BH on the ceramic membrane's architecture is clearly evident. The SEM image demonstrates the formation of pores in the $C_{77}S_{20}BH_3$-T_{950} membrane, which are attributed to the presence of BH. During pyrolysis, BH transforms from its organic state into carbon [9, 29, 44, 57]. In the sintered $C_{77}S_{20}BH_3$ membrane, the black particles observed are likely carbonized remnants of BH following sintering at 950°C. Consequently, the pore size increases due to the thermal decomposition of the soft segments of BH within the membrane matrix [21, 29, 41, 57]. As highlighted in Figure 6c, the pores of the $C_{77}S_{20}BH_3$-T_{950} membrane exhibit variable diameters, predominantly smaller than 50 µm. Moreover, the residual carbon from BH pyrolysis may be advantageous, as it can provide active sites for pollutant adsorption during wastewater treatment [21, 58]. Similar observations have been reported when using plant-derived materials as pore-forming agents to enhance the porosity and permeability of clay-based ceramic membranes [21, 48, 57].

3.4.2 | Analysis of AFM

The surface topography of the fabricated ceramic membranes was analyzed using AFM. Based on the AFM data, both the thickness of the selective layer and the surface roughness of the produced membranes were determined. Figure 7 presents the three-dimensional AFM micrographs of the $C_{77}S_{20}BH_3$-T_{950} ceramic membranes. Although AFM can only scan a limited area, the results reveal that the obtained GTCMs possess a relatively rough surface, which is beneficial for enhancing adhesion. Consequently, the increased surface roughness of the membranes enhances their potential for particle capture [59]. Generally, a

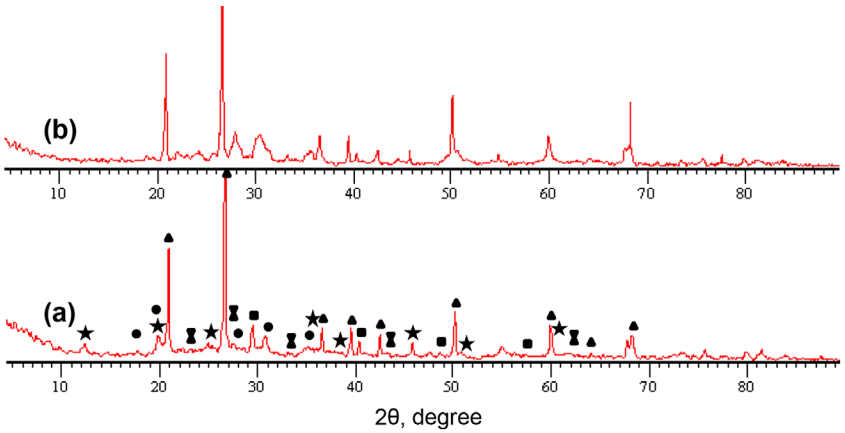

FIGURE 8 | XRD diffractograms of: (a) Libyan kaolin clay and (b) $C_{77}S_{20}BH_3$-T_{950} membrane. (★: Kaolinite, ▲: Quartz, ■: Calcite, ●: Muscovite, ⧗: Lepidocrocite).

higher degree of surface roughness contributes to an enlarged surface area and improved hydrophilicity of the membrane [44].

3.4.3 | Analysis of XRD

The mineralogical analysis of the neat LKC and $C_{77}S_{20}BH_3$-T_{950} ceramic membrane was also evaluated using XRD (see Figure 8). The results indicated that the LKC, used as the starting material for the ceramic membrane, contained various minerals. This LKC primarily consisted of common clay minerals, with kaolin being the dominant component, as evidenced by multiple peaks in the x-ray diffractogram at $2\theta = 12.27°$, 19.92°, and 35.01°. Minor impurities, including quartz ($2\theta = 20.86°$, 26.63°, 42.44°) and calcite ($2\theta = 29.36°$, 39.49°, 48.63°), were also detected in smaller amounts. Additionally, muscovite was present, showing characteristic peaks at $2\theta = 8.83°$, 19.81°, and 31.04°. Lepidocrocite ($2\theta =$ 22.43°, 26.97°, 43.25°) was also observed [30]. The XRD analysis of the $C_{77}S_{20}BH_3$-T_{950} ceramic membrane reveals notable changes compared to the raw LKC. The characteristic peaks of kaolinite ($2\theta = 12.27°, 19.92°, 35.01°$) are no longer detectable after sintering at 950°C, indicating the transformation of kaolinite to metakaolin and eventually to amorphous or crystalline phases such as mullite. The quartz peaks ($2\theta = 20.86°$, 26.63°, 42.44°) remain prominent after sintering. However, it should be noted that without quantitative phase analysis (e.g., Rietveld refinement or internal standard method), we cannot unequivocally conclude an absolute increase in quartz content; the relative peak intensities may also be influenced by the loss or transformation of other phases. Regarding calcite ($2\theta = 29.36°, 39.49°, 48.63°$), its characteristic peaks are no longer clearly distinguishable in the sintered membrane, suggesting that calcite has largely decomposed (as expected at temperatures above 800°C) or that its remaining crystalline domains are below the detection limit of XRD. Some peak broadening in this region may also indicate partial overlap with other phases [4]. Comparable structural changes have been observed in other clay-based ceramic membranes [4, 30].

3.4.4 | Mechanical Properties of the Membranes

The effect of sintering temperature on the mechanical strength of the fabricated ceramic membrane ($C_{77}S_{20}BH_3$) was further

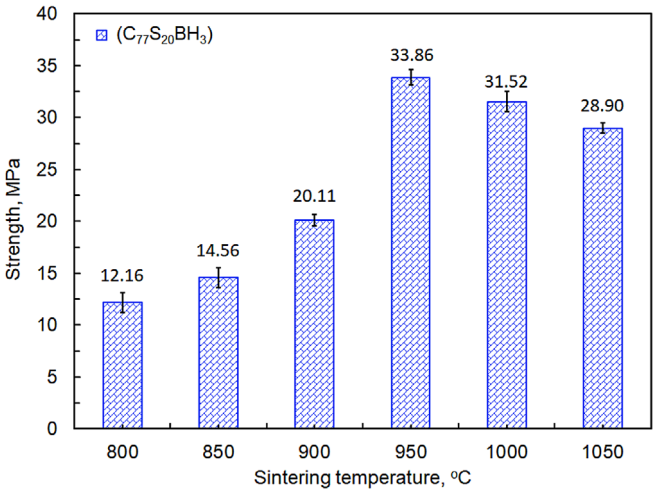

FIGURE 9 | Mechanical strength of $C_{77}S_{20}BH_3$ ceramic membranes at different sintering temperatures.

investigated (Figure 9). The results indicated that the sintering temperature has a significant influence on the membrane strength. For $C_{77}S_{20}BH_3$ ceramic membrane, the mechanical strength values were increased from 12.16 to 20.24 MPa with an increase in the sintering temperature from 800°C to 900°C. The increase in the membrane strength is attributed to the raise of grain growth process that led to a membrane densification [26, 42]. The highest mechanical strength value of 33.86 MPa was achieved for the optimized $C_{77}S_{20}BH_3$ membrane sintered at 950°C. When the temperature was further increased to 1000°C–1050°C, the mechanical strength slightly decreased to 31.52 and 28.90 MPa, respectively. This decline is attributed to over-sintering effects, including excessive grain coarsening and the formation of micro-cracks due to differential thermal expansion between different mineral phases [60]. The rise in the sintering temperature can result in more densely packed ceramic particle grain achieved, which can lower the membrane porosity and enhance the membrane strength. However, beyond 950°C, the negative effects of over-sintering outweigh the benefits of further densification. A similar observation was reported for ceramic membranes that sintered at 950°C give the highest mechanical strength [42, 45]. Although sintering at 1000°C still yields rela-

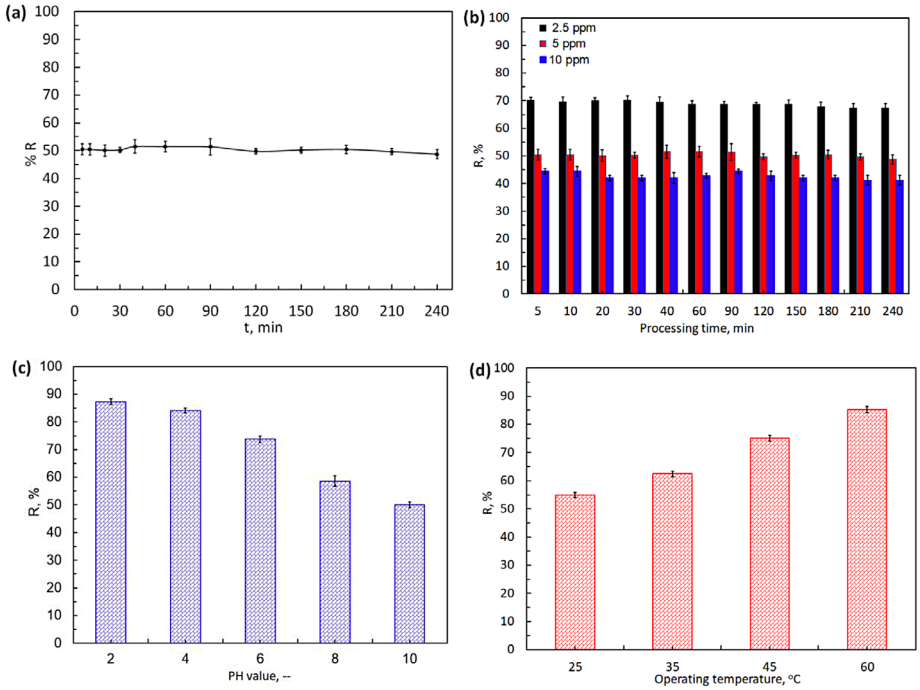

FIGURE 10 | Rejection efficiency values of Cr(VI) using the$C_{77}S_{20}BH_3$ceramic membranes: (a, b) Effect the processing time (pH 8 and initial concentration of 5 ppm). (c) Effect of the initial concentration (pH=8). (d) Effect of the operating temperature (pH= 8 and initial concentration of 2.5 ppm).

tively high mechanical strength (31.52 MPa), the corresponding decrease in porosity and increase in shrinkage lead to lower water permeability, confirming 950°C as the optimal sintering temperature. Furthermore, the results demonstrated that $C_{77}S_{20}BH_3$-T_{950} membrane has excellent mechanical strength. Consequently, this optimized membrane is recommended to be used in practical applications.

3.5 | Chromium Rejection Study

The $C_{77}S_{20}BH_3$-T_{950} ceramic membrane was evaluated for Cr(VI) removal from water. As shown in Figure 10a, the Cr(VI) removal from aqueous solutions. Cr(VI) was selected as a model heavy metal contaminant due to its high toxicity, mobility, and prevalence in industrial effluents. The removal mechanism involves a combination of electrostatic adsorption, size exclusion, and surface complexation, given the membrane's porous structure (mean pore size ~56 nm) and the presence of surface functional groups (Si–OH, Al–OH, Fe–OH) derived from clay minerals [35, 61]. As shown in Figure 10a, the Cr(VI) removal efficiency was monitored over time at an initial concentration of 5 ppm, pH 8, and room temperature. The membrane achieved a maximum removal efficiency of 52.64%, with only a slight decrease to 48.73% after 4 h, indicating good operational stability.

A comparative analysis of the $C_{77}S_{20}BH_3$-T_{950} membrane with other low-cost clay-based ceramic membranes reported in the literature is presented in Table 5. The results show that our membrane exhibits a competitive Cr(VI) rejection of 87.2% while maintaining a high water permeability of ~476 $L.h^{-1}.m^{-2}.bar^{-1}$. For instance, a Tunisian kaolin membrane achieved a comparable rejection (~85%) but with a much lower permeability (21.2 $L.h^{-1}.m^{-2}.bar^{-1}$) [17]. A Moroccan clay/banana peel membrane showed higher permeability (550 $L.h^{-1}.m^{-2}.bar^{-1}$) but lower Cr(VI) rejection (~70%) [31]. Although a rice husk ash/kaolin hollow fiber membrane exhibited higher permeability (675 $L.h^{-1}.m^{-2}.bar^{-1}$), its rejection was slightly lower (82%), and it required a higher sintering temperature (1100°C) [21]. Thus, the GTCM developed in this study offers an excellent trade-off between flux, selectivity, and energy cost, making it a promising candidate for sustainable wastewater treatment.

3.5.1 | Effect of Initial Concentration

Figure 10b presents the effect of initial Cr(VI) concentration on rejection performance. Maximum rejection rates of 70.08%, 52.64%, and 44.40% were observed for initial concentrations of 2.5, 5, and 10 ppm, respectively. The inverse relationship between initial concentration and rejection efficiency can be explained by the limited availability of surface adsorption sites on the membrane. At higher concentrations, the fixed number of active sites becomes saturated more rapidly, and the increased concentration gradient across the membrane drives a higher diffusive flux of Cr(VI) species through the porous structure. Additionally, the electrostatic repulsion between adsorbed anionic Cr(VI) species and incoming ions becomes more pronounced at higher surface loadings, further reducing net rejection. These trends are consistent with previous reports on clay-based membranes for heavy metal removal [4, 8, 62]. Notably, after 4 h of operation, rejection efficiency decreased only slightly (by approximately 1.48%–2.98%) across all concentrations, demonstrating that the membrane maintains stable performance over time without significant fouling or saturation under these conditions.

TABLE 5 | Comparative study of low-cost clay-based ceramic membranes for Cr(VI) removal.

Raw material	Sintering Temp. (°C)	Pore size (μm)	Porosity (%)	Permeability ($L.h^{-1}.m^{-2}.bar^{-1}$)	Cr(VI) Rejection (%)	Ref.
Libyan kaolin/sand/BH[a]	950	0.056	34.3	476	87.2	This study
Tunisian kaolin	1000	0.035	26.0	21.2	~85	[17]
Rice husk ash/kaolin (HF)[b]	1100	0.045	38.0	675	82	[21]
Moroccan red clay/BP[c]	1100	5.500	40.0	550	~70	[31]

[a]BH: Barely husk.
[b]BP: banana peel.
[c]HF: Hollow fiber.

3.5.2 | Effect of pH

The influence of initial solution pH on Cr(VI) removal was examined over a range of pH 2.0 to 10.0 (Figure 10c). Cr(VI) rejection was strongly pH-dependent, increasing significantly under acidic conditions: from 58.62% at pH 8 to 84.14% at pH 4, and reaching a maximum of 87.24% at pH 2. This behavior is governed by two interrelated chemical factors: (i) the speciation of Cr(VI) in aqueous solution, and (ii) the surface charge of the ceramic membrane.

(i) Speciation of Cr(VI): In aqueous solutions, Cr(VI) exists in different anionic forms depending on pH. At pH > 6, the dominant species is chromate (CrO_4^{2-}). In the pH range 2–6, the predominant species is hydrogen chromate ($HCrO_4^-$), while at pH < 2, dichromate ($Cr_2O_7^{2-}$) and neutral chromic acid (H_2CrO_4) may form. The degree of protonation influences both the charge density and the affinity for adsorption sites.

(ii) Membrane surface charge: The surface of the $C_{77}S_{20}BH_3$-T_{950} membrane contains abundant hydroxyl groups (–OH) bonded to silicon (Si–OH), aluminum (Al–OH), and iron (Fe–OH) atoms, derived from kaolin clay and sand. The protonation state of these groups is pH-dependent: under acidic conditions (low pH), the surface hydroxyl groups become protonated, creating a positively charged membrane surface, whereas under basic conditions (high pH), deprotonation occurs, resulting in a negatively charged surface [9].

Since Cr(VI) exists as anionic species ($HCrO_4^-$, CrO_4^{2-}, and $Cr_2O_7^{2-}$) under most environmental conditions, the positively charged surface at low pH strongly attracts these anions via electrostatic interactions, promoting adsorption and subsequent rejection. Conversely, at high pH, electrostatic repulsion between the negatively charged membrane surface and anionic Cr(VI) species reduces rejection efficiency. The maximum rejection of 87.24% at pH 2 is attributed to the combination of: (i) maximum positive surface charge density, (ii) favorable speciation (predominantly $HCrO_4^-$and $Cr_2O_7^2$, which have higher charge-to-size ratios), and (iii) potential surface complexation reactions where Cr(VI) species bind directly to surface metal centers. These results are in excellent agreement with earlier studies on clay-based ceramic membranes, where optimal Cr(VI) removal was consistently observed at pH 2–3 [21, 58, 63].

3.5.3 | Effect of Temperature

The influence of operating temperature on Cr(VI) rejection was investigated over a range of 25°C to 60°C under fixed conditions (initial concentration 5 ppm, pH 2, pressure 3 bar). As shown in Figure 10d, the rejection efficiency increased progressively with temperature, rising from 54.94% at 25°C to 85.23% at 60°C. This positive temperature dependence can be attributed to several interrelated mechanisms. First, elevated temperatures reduce water viscosity and increase the diffusion coefficient of Cr(VI) species, thereby enhancing their transport toward the membrane surface; more importantly, higher temperatures improve the kinetics of surface interactions, which play a dominant role in the rejection process. Second, thermal energy increases the mobility and reactivity of surface hydroxyl groups (≡Si–OH, ≡Al–OH), promoting more efficient protonation/deprotonation equilibria and fostering chemisorption of Cr(VI) onto the membrane surface. Third, higher temperatures reduce both the thickness and hydraulic resistance of the concentration polarization layer adjacent to the membrane surface, allowing more effective contact between Cr(VI) species and available adsorption sites. Additionally, although the ceramic membrane is thermally stable (sintered at 950°C), minor and reversible changes in surface hydration states at 60°C may further enhance affinity toward Cr(VI) species. While increased rejection at higher temperatures is advantageous, the associated energy costs must be considered for practical applications. Nevertheless, the observed performance (85.23% at 60°C) demonstrates that the membrane is highly effective for Cr(VI) removal under moderately elevated temperatures, making it particularly suitable for treating industrial effluents that are discharged hot [64, 65].

3.5.4 | Comparison With Literature and Mechanistic Summary

In summary, the monolayer $C_{77}S_{20}BH_3$-T_{950} membrane achieves a Cr(VI) removal performance (R = 87.24% at pH 2) that is comparable to more complex composite systems, such as the Sm/Z6 UF membrane, which consists of six layers of smectite nanoparticles deposited on a zeolite support and exhibits 89%

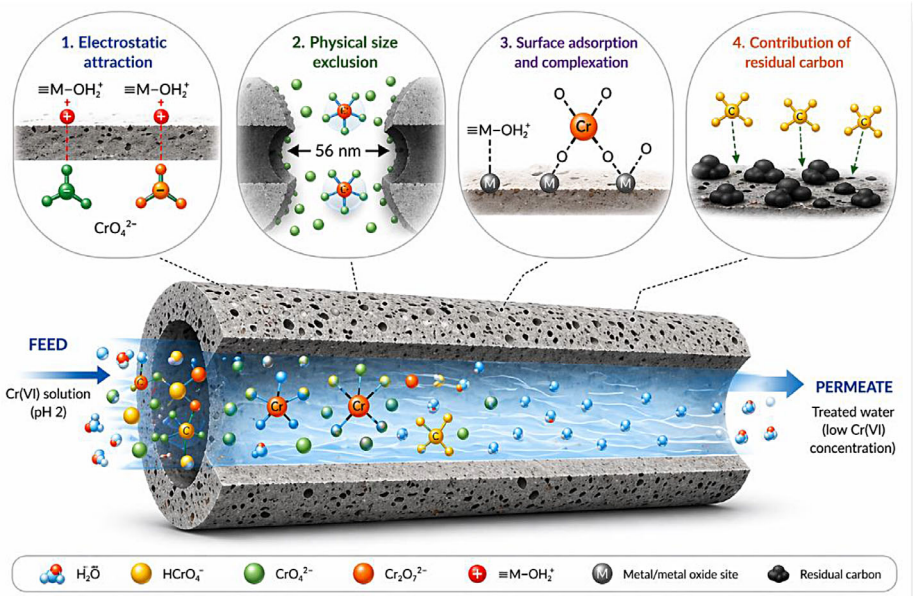

FIGURE 11 | Proposed Cr(VI) rejection mechanism of the $C_{77}S_{20}BH_3$-T_{950} ceramic membrane.

removal at pH 2.9 [9]. However, the membrane developed in this study offers a significant advantage as it is fabricated via a single-step extrusion process, whereas Sm/Z6 requires multiple coating layers; the absence of a separate active layer minimizes mass transfer resistance, contributing to the high permeability of ~476 $L{\cdot}h^{-1}{\cdot}m^{-2}{\cdot}bar^{-1}$. The overall Cr(VI) rejection mechanism is therefore described as a synergistic process involving electrostatic attraction between positively charged surface sites ($\equiv M{-}OH_2^+$) and anionic Cr(VI) species ($HCrO_4^-$, CrO_4^{2-}, $Cr_2O_7^{2-}$) under acidic conditions, combined with physical size exclusion by the 56 nm porous structure that partially restricts the passage of hydrated Cr(VI) ions whose hydrated diameter is approximately 0.5–0.8 nm, though larger clusters or aggregates may also form. This mechanism is further complemented by surface adsorption followed by possible surface complexation, particularly at low pH where metal–oxygen–chromium bonds can form, as well as a minor contribution from residual carbon derived from BH pyrolysis, which may provide additional hydrophobic adsorption sites for Cr(VI) species. This multi-mechanistic framework consistently explains the strong pH dependence, the inverse relationship between rejection efficiency and initial concentration, and the positive temperature effect observed throughout this study.

3.6 | Membrane Regeneration

The membranes gradually lose their ability to separate components from the feed solutions during filtration. There is a noticeable deterioration of the membrane surface along with this fouling [66]. After treatment of the chromium aqueous solution at optimized conditions (initial concentration of 2.5 ppm and pH 2), the results confirmed intensive membrane fouling (>26%). In fact, it is clear from Figure 12 that the permeate flux of the $C_{77}S_{20}BH_3$-T_{950} membrane before cleaning is less than the water permeate flux due to pore blocking and the formation of a polarization layer on the membrane surface. For this reason, to recover the initial membrane performance, a chemical cleaning procedure was required [67]. The water permeability was measured to

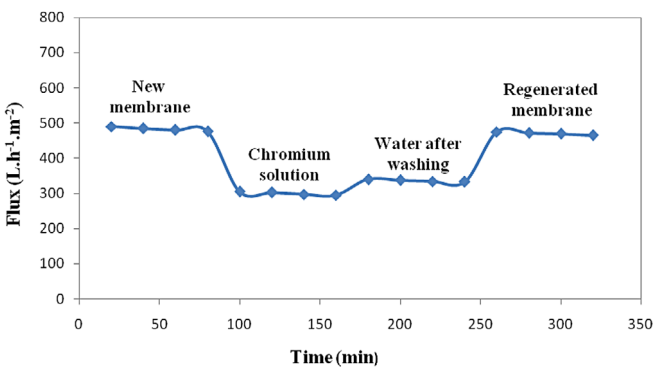

FIGURE 12 | Recovery of $C_{77}S_{20}BH_3$-T_{950} membrane performance after acid–base cleaning procedure.

estimate the effectiveness of the membrane regeneration. The results showed that the water permeability values were extremely close, verifying the cleaning process's efficacy (Figures 11 and 12). After chemical cleaning, the FRR was found to be approximately 70%, indicating partial restoration of membrane permeability. This suggests that while the cleaning protocol is effective, some irreversible fouling occurs, likely due to strong adsorption of Cr(VI) ions.

3.7 | Cost Estimation

The economic viability of membrane production was analyzed by evaluating expenditures on raw materials and energy consumption. Conventional membranes composed of high-purity metallic oxides (e.g., alumina, zirconia) are notably costly, with prices reported by Abdullayev et al. [68] in the range of $500–$1,000/m^2. This high cost is attributed to the use of valuable precursor materials and the substantial energy input needed for sintering at high temperatures. For comparison, the specific cost components of a kaolin-based membrane encompassing material

TABLE 6 | Details of cost estimation for the fabrication of the $C_{77}S_{20}BH_3$ membrane.

Cost of raw materials			
Material	**Unit per Kg ($)**	**Amount of raw material (g)**	**Price ($)**
Libyan kaolin powder	0.16	308	0.0493
Natural sand powder	0.029	80	0.0023
Distilled water	0.28	200	0.056
barley husks	—	12	—
Total raw materials cost for the fabrication of 15 membranes			0.1076
Energy cost (Based on the power consumption)			
Mixer			0.031
Dry oven			0.027
Extruder			0.138
Furnace			0.086
Total production cost for the fabrication of 15 membranes ($)			0.3896
(Surface of membrane = 1.7×10^{-3} m^2)			
Total production cost of the $C_{77}S_{20}BH_3$ membrane ($.$m^{-2}$)			15.27

procurement and modification, shaping, and sintering energy are described in Table 6.

The developed sustainable ceramic membrane demonstrates remarkable cost-effectiveness, priced at \$15.27/m^2, which gives it a significant competitive edge for wastewater treatment. A comparative cost analysis highlights substantial savings against several benchmarks: it is 13% less expensive than zeolite/smectite membranes (\$17.56/m^2) [45], offers savings of 24%–27% compared to kaolin/zeolite composites (\$20.92/m^2) [1] and surface-modified zeolite systems (\$20.11/m^2) [69], and represents a cost reduction exceeding 86% over more expensive alternatives derived from agricultural waste, such as walnut shell/kaolin membranes, which can cost over \$112/m^2 [70]. Furthermore, it shows a slight 4% improvement over a kaolin/almond shell/lime composition (\$15.97/m^2) [23]. Crucially, these economic advantages are achieved without compromising separation performance, confirming the membrane's technical viability and superior cost-effectiveness compared to other ceramic membranes based on natural materials.

4 | Conclusions

An eco-friendly tubular ceramic membrane was successfully fabricated from LKC modified with BH and sintered at 950°C. This membrane exhibited a highly porous structure (34.28% porosity, average pore size of 5.64×10^{-2} µm), enabling relative high water permeability (~476 $L.h^{-1}.m^{-2}.bar^{-1}$), along with strong mechanical properties and excellent chemical stability. The $C_{77}S_{20}BH_3$-T_{950} membrane demonstrated outstanding performance in removing Cr(VI), with efficiency strongly influenced by solution conditions. A maximum rejection rate of 87.2% was achieved at pH 2 for an initial Cr(VI) concentration of 2.5 ppm, while higher concentrations led to reduced removal efficiency. From an economic standpoint, the novel membrane was estimated at a cost of 15.27$.$m^{-2}$, demonstrating significant cost-effectiveness compared to conventional ceramic membranes. Furthermore, chemical cleaning protocols proved fully effective in restoring the membrane's initial permeability, ensuring sustainable long-term performance. Produced from low-cost natural materials, this membrane offers a sustainable, robust, and promising approach for wastewater treatment applications, particularly for the removal of heavy metals such as chromium.

Acknowledgments

The authors are grateful to the Ministry of Education of Tunisia for the financial support in the form of an international scholarship awarded to Mr. Mhamed A. Aburawi. The authors acknowledge Dr. Mohammed Ghath, Misurata University, for his kind help in the FTIR measurements.

Open Access funding enabled and organized by CNUDST.

Conflicts of Interest

The authors declare no conflicts of interest.

Data Availability Statement

The data that support the findings of this study are available from the corresponding author upon reasonable request.

References

1. H. Aloulou, W. Aloulou, J. Duplay, L. Baklouti, L. Dammak, and R. B. Amar, "Development of Ultrafiltration Kaolin Membranes Over Sand and Zeolite Supports for the Treatment of Electroplating Wastewater," *Membranes* 12, no. 11 (2022): 1066, https://doi.org/10.3390/membranes12111066.

2. S. Jana, M. K. Purkait, and K. Mohanty, "Preparation and Characterization of Low-Cost Ceramic Microfiltration Membranes for the Removal of Chromate From Aqueous Solutions," *Applied Clay Science* 47, no. 3-4 (2010): 317–324, https://doi.org/10.1016/j.clay.2009.11.036.

3. R. V. Kumar, A. K. Ghoshal, and G. Pugazhenthi, "Elaboration of Novel Tubular Ceramic Membrane From Inexpensive Raw Materials by

Extrusion Method and Its Performance in Microfiltration of Synthetic Oily Wastewater Treatment," *Journal of Membrane Science* 490 (2015): 92–102, https://doi.org/10.1016/j.memsci.2015.04.066.

4. S. Saja, A. Bouazizi, B. Achiou, et al., "Fabrication of Low-Cost Ceramic Ultrafiltration Membrane Made From Bentonite Clay and Its Application for Soluble Dyes Removal," *Journal of the European Ceramic Society* 40 (2020): 2453–2462, https://doi:10.1016/j.jeurceramsoc.2020.01.057.

5. R. B. Amar, W. Aloulou, H. Aloulou, and A. Attia, "Treatment of Wastewater From Electroplating Industry Using Low-Cost Ceramic Membranes," in *Application of Low Cost Ceramic Membranes in Wastewater Treatment, Materials Horizons: From Nature to Nanomaterials*, ed. S. Bandyopadhyay (Springer Nature Singapore Pte Ltd, 2025), 157–169, https://doi.org/10.1007/978-981-97-5842-5_6.

6. S. Roy, S. Majumda, G. C. Sahoo, A. K. Mandal, N. Dey, and P. Mondal, "Preparation of Stable and Regenerable Ceramic-Supported-Polymeric Composite Nanofiltration Membrane With High Flux and Heavy Metal Removal Performance," *Journal of Water Process Engineering* 59 (2024): 104940, https://doi:10.1016/j.jwpe.2024.104940.

7. N. Dizge, Y. Ozay, M. Boussemghoune, and M. Chikhi, "Preparation of Catalytic Polyether Sulfone Coated Ceramic Membrane for Reduction of Hexavalent Chromium," *Journal of Water Process Engineering* 40 (2021): 101946, https://doi.org/10.1016/j.jwpe.2021.101946.

8. H. Zhu, J. Yuan, X. Tan, W. Zhang, M. Fang, and X. Wang, "Efficient Removal of Pb^{2+} by Tb-MOFs: Identifying the Adsorption Mechanism Through Experimental and Theoretical Investigations," *Environmental Science: Nano* 6 (2019): 261–272, https://doi:10.1039/C8EN01066.

9. W. Aloulou, H. Aloulou, M. Khemakhem, J. Duplay, M. O. Daramola, and R. B. Amar, "Synthesis and Characterization of Clay-Based Ultrafiltration Membranes Supported on Natural Zeolite for Removal of Heavy Metals From Wastewater," *Environmental Technology & Innovation* 18 (2020): 100794, https://doi.org/10.1016/j.eti.2020.100794.

10. M. Khemakhem, S. Khemakhem, S. Ayedi, M. Cretin, and R. B. Amar, "Development of an Asymmetric Ultrafiltration Membrane Based On Phosphates Industry Sub-Products," *Ceramics International* 41 (2015): 10343–10348, https://doi:10.1016/j.ceramint.2015.05.101.

11. A. Nouri, S. F. Chua, E. Mahmoudi, A. W. Mohammad, and W. L. Ang, "Fabrication of Graphene Oxide Decorated With Poly(dimethyl amino ethyl methacrylate) Brush for Efficient Cr(VI) Adsorption From Aqueous Solution," *Chinese Journal of Chemical Engineering* 73 (2024): 51–61, https://doi:10.1016/j.cjche.2024.03.030.

12. Y. Shi, X. Wang, S. Zhong, W. Chen, C. Feng, and S. Yang, "Nano Zero-Valent Iron/Montmorillonite Composite for the Removal of Cr(VI) From Aqueous Solutions: Characterization, Performance, and Mechanistic Insights," *Applied Clay Science* 253 (2024): 107345, https://doi:10.1016/j.clay.2024.107345.

13. World Health Organization , *Guidelines for Drinking-water Quality, 4th ed., incorporating Ist addendum* (WHO Press, 2017), https://www.who.int/publications/i/item/9789241549950.

14. U. S. Environmental Protection Agency, National Primary Drinking Water Regulations: Chromium, EPA 816-F-20-001 (2020), https://www.epa.gov/ground-water-and-drinking-water/national-primary-drinking-water-regulations.

15. Norme Tunisienne NT 106.002, *Protection De L' Environnement—Rejets d' Effluents Dans Le milieu hydrique*, (INRST, 2018).

16. W. J. Ang, Y. H. Teow, Z. H. Chang, A. W. Mohammad, and T. W. Wan, "Innovative Ceramic Membrane Plate Filtration System for Sustainable Semiconductor Industry Wastewater Treatment: A Pilot Scale Study," *Chemical Engineering Journal* 496 (2024): 153767, https://doi.org/10.1016/j.cej.2024.153767.

17. S. Bousbih, E. Errais, F. Darragi, et al., "Treatment of Textile Wastewater Using Monolayered Ultrafiltation Ceramic Membrane Fabricated From Natural Kaolin Clay," *Environmental Technology* 42, no. 21 (2021): 3348–3359, https://doi.org/10.1080/09593330.2020.1729242.

18. N. M. A. Omar, M. H. D. Othman, Z. S. Tai, et al., "Recent Strategies for Enhancing the Performance and Lifespan of Low-Cost Ceramic Membranes in Water Filtration and Treatment Processes: A Review," *Journal of Water Process Engineering* 62 (2024): 105399, https://doi:10.1016/j.jwpe.2024.105399.

19. D. E. Idrissi, Z. C. Elidrissi, B. Achiou, M. Ouammou, and S. A. Younssi, "Fabrication of Low-Cost Kaolinite/Perlite Membrane for Microfiltration of Dairy and Textile Wastewaters," *Journal of Environmental Chemical Engineering* 11 (2023): 109281, https://doi.org/10.1016/j.jece.2023.109281.

20. D. O. Obada, D. Dodoo-Arhin, M. Dauda, F. O. Anafi, A. S. Ahmed, and O. A. Ajayi, "Physico-Mechanical and Gas Permeability Characteristics of Kaolin Based Ceramic Membranes Prepared With a New Pore-Forming Agent," *Applied Clay Science* 150 (2017): 175–183, https://doi:10.1016/j.clay.2017.09.014.

21. S. K. Hubadillah, M. H. D. Othman, Z. Harun, A. Ismail, M. A. Rahman, and J. Jaafar, "A Novel Green Ceramic Hollow Fiber Membrane (CHFM) Derived From Rice Husk Ash as Combined Adsorbent-Separator for Efficient Heavy Metals Removal," *Ceramics International* 43 (2017): 4716–4720, https://doi.org/10.1016/j.ceramint.2016.12.122.

22. P. Kamgang-Syapnjeu, D. Njoya, E. Kamseu, et al., "Elaboration of a New Ceramic Membrane Support From Cameroonian Clays, Coconut Husks and Eggshells: Application for *Escherichia coli* Bacteria Retention," *Applied Clay Science* 198 (2020): 105836, https://doi:10.1016/j.clay.2020.105836.

23. J. Bahrouni, A. Attia, F. Z. Elberrichi, et al., "Green and Sustainable Clay Ceramic Membrane Preparation and Application to Textile Wastewater Treatment for Color Removal," *Membranes* 15 (2025): 292, https://doi.org/10.3390/membranes15100292.

24. A. El Azizi, A. Bayoussef, C. Bai, et al., "Development of Clayey Ceramic Membranes Prepared With Bio-Based Additives: Application in Water and Textile Wastewater Treatment," *Ceramics International* 49 (2023): 5776–5787, https://doi.org/10.1016/j.ceramint.2022.10.094.

25. W. Aloulou, H. Aloulou, M. Romdhani, L. Dammak, and R. B. Amar, "Effectiveness Evaluation of a Flat Smectite Membrane for Wastewater Purification: Characterization, Cost and Energy Estimation," *Desalination and Water Treatment* 318 (2024): 100390, https://doi.org/10.1016/j.dwt.2024.100390.

26. Y. Khmiri, A. Attia, H. Aloulou, L. Dammak, L. Baklouti, and R. B. Amar, "Preparation and Characterization of New and Low-Cost Ceramic Flat Membranes Based on Zeolite-Clay for the Removal of Indigo Blue Dye Molecules," *Membranes* 13, no. 11 (2023): 865, https://doi:10.3390/membranes13110865.

27. H. Aloulou, H. Bouhamed, R. B. Amar, and S. Khemakhem, "New Ceramic Microfiltration Membrane From Tunisian Natural Sand: Application for Tangential Wastewater Treatment," *Desalination and Water Treatment* 78 (2017): 41–48, https://doi.org/10.5004/dwt.2017.20921.

28. L. Hamoudi, D. E. Akretche, A. Hadadi, A. Amrane, and L. Mouni, "Comparative Study of Ceramic Membranes Developed on Different Algerian Natural Clays for Industrial-Effluent Filtration," *Minerals* 13, no. 2 (2023): 273, https://doi.org/10.3390/min13020273.

29. M. Rafya, W. Misrar, L. Saâdi, et al., "Ceramic Membrane Support Based on Kaolin and Solid Waste From Hydrodistillation of *Rosmarinus officinalis L*," *Materials Chemistry and Physics* 295 (2023): 127030, https://doi:10.1016/j.matchemphys.2022.127030.

30. M. Mouiya, A. Abourriche, A. Bouazizi, et al., "Flat Ceramic Microfiltration Membrane Based on Natural Clay and Moroccan Phosphate for Desalination and Industrial Wastewater Treatment," *Desalination* 427 (2018): 42–50, https://doi:10.1016/j.desal.2017.11.005.

31. M. Mouiya, A. Bouazizi, A. Abourriche, et al., "Fabrication and Characterization of a Ceramic Membrane From Clay and Banana Peel Powder: Application to Industrial Wastewater Treatment," *Materials Chemistry and Physics* 227 (2019): 291–301, https://doi:10.1016/j.matchemphys.2019.02.011.

32. Y. Li, Y. Ma, J. Dai, Z. Ye, and L. Wu, "Nanofiltration Membrane With Surface Nanostructure Induced by Interfacial Modification for Heavy Metal Ions Removal, Salt Selection and Antibacterial," *Journal of Environmental Chemical Engineering* 2, no. 2 (2024): 112439, https://doi.org/10.1016/j.jece.2024.112439.

33. C. I. Covaliu-Mierlă, O. Păunescu, and H. Iovu, "Recent Advances in Membranes Used for Nanofiltration to Remove Heavy Metals From Wastewater: A Review," *Membranes* 13, no. 7 (2023): 643, https://doi.org/10.3390/membranes13070643.

34. M. Dawam, M. Gobara, H. Oraby, M. Y. Zorainy, and I. M. Nabi, "Advances in Membrane Technologies for Heavy Metal Removal From Polluted Water: A Comprehensive Review," *Water, Air, & Soil Pollution* 236 (2025): 461, https://doi.org/10.1007/s11270-025-08035-6.

35. H. Aloulou, A. Attia, F. Aouay, et al., "Functional Material Innovations in Ultrafiltration and Microfiltration for Advanced Water Treatment: A Comprehensive Review," *Environmental Science: Water Research & Technology* 12 (2026): 1670–1692, https://doi.org/10.1039/D6EW00201C.

36. R. Shoshaa, M. Y. Ashfaq, and M. A. Al-Ghouti, "Recent Developments in Ultrafiltration Membrane Technology for the Removal of Potentially Toxic Elements, and Enhanced Antifouling Performance: A Review," *Environmental Technology & Innovation* 31 (2023): 103162, https://doi.org/10.1016/j.eti.2023.103162.

37. A. M. Nasir, P. S. Goh, M. S. Abdullah, B. C. Ng, and A. F. Ismail, "Adsorptive Nanocomposite Membranes for Heavy Metal Remediation: Recent Progresses and Challenges," *Chemosphere* 232 (2019): 96–112, https://doi.org/10.1016/j.chemosphere.2019.05.174.

38. Z. Samavati, A. Samavati, P. S. Goh, A. F. Ismail, and M. S. Abdullah, "A Comprehensive Review of Recent Advances in Nanofiltration Membranes for Heavy Metal Removal From Wastewater," *Chemical Engineering Research and Design* 189 (2023): 530–571, https://doi.org/10.1016/j.cherd.2022.11.042.

39. M. D. Alsubei, B. Reid, S. A. Aljlil, M.-O. Coppens, and L. C. Campos, "Fabrication and Characterization of Coated Ceramic Membranes From Natural Sources for Water Treatment Applications," *Journal of Membrane Science* 690 (2024): 122226, https://doi.org/10.1016/j.memsci.2023.122226.

40. L. Sawunyama, O. A. Oyewo, M. F. Bopape, and D. C. Onwudiwe, "Fabrication and Characterization of Low-Cost Ceramic Membranes From Coal Fly Ash and Natural Sand," *Sustainable Chemistry for the Environment* 8 (2024): 100165, https://doi:10.1016/j.scenv.2024.100165.

41. S. Njuhou, M. Mouafon, A. Pountouenchi, O. R. Njindam, G. L. Lecomte-Nana, and D. Njoya, "Rice Husks and Kaolin Based Ceramic Membrane for Filtration of Slaughterhouse Wastewater: Optimization Study Using Response Surface Methodology (RSM) and Responses Interdependence Analysis," *Transactions of the Indian Ceramic Society* 82 (2023): 143–155, https://doi:10.1080/0371750X.2023.2205601.

42. N. Malik, V. K. Bulasara, and S. Basu, "Preparation of Novel Porous Ceramic Microfiltration Membranes From Fly Ash, Kaolin and Dolomite Mixtures," *Ceramics International* 46 (2020): 6889–6898, https://doi:10.1016/j.ceramint.2019.11.184.

43. A. A. Alhwaige, H. Ishida, and S. Qutubuddin, "Chitosan/Polybenzoxazine/Clay Mixed Matrix Composite Aerogels: Preparation, Physical Properties, and Water Absorbency," *Applied Clay Science* 184 (2020): 105403, https://doi.org/10.1016/j.clay.2019.105403.

44. O. T. Mahlangu, G. Mamba, and B. B. Mamba, "A Facile Synthesis Approach for GO-ZnO/PES Ultrafiltration Mixed Matrix Photocatalytic Membranes for Dye Removal in Water: Leveraging the Synergy Between Photocatalysis and Membrane Filtration," *Journal of Environmental Chemical Engineering* 11 (2023): 110065, https://doi:10.1016/j.jece.2023.110065.

45. Y. Khmiri, A. Attia, N. Elboughdiri, et al., "Preparing Sustainable Membranes Made From Zeolite–Smectite for Treating Textile Wastewater and Pulp Industry Wastewater," *ChemistrySelect* 2024, 9, e202404190, https://doi.org/10.1002/slct.202404190.

46. M. Hashim, S. Mukhopadhyay, J. N. Sahu, and B. Sengupta, "Remediation Technologies for Heavy Metal Contaminated Groundwater," *Journal of Environmental Management* 92 (2011): 2355–2388, https://doi.org/10.1016/j.jenvman.2011.06.009.

47. Z. Salah, H. Aloulou, W. Aloulou, C. Algieri, S. M. Chergui, and R. B. Amar, "Development of Graphene Oxide Membrane on Flat Mud Ceramic Support for Methylene Blue Dyes Removal," *ChemistrySelect* 10 (2025): e202406142, https://doi.org/10.1002/slct.202406142.

48. S. Foorginezhad and M. Zerafat, "Microfiltration of Cationic Dyes Using Nano-Clay Membranes," *Ceramics International* 43 (2017): 15146–15159, https://doi.org/10.1016/j.ceramint.2017.08.045.

49. A. A. Alhwaige, A. N. Al-Drogi, M. B. Yahiya, and W. K. Elhrari, "Mixed Matrix Membranes-Derived From High-Density Polyethylene and Mesembryanthemum Crystallinum for Separation of Methylene Blue Dye From Aqueous Solutions," *Journal of Marine Science & Environmental Technology* 1, no. 2 (2025): 1–19, https://doi.org/10.59743/jmset.v10i2.185.

50. S. Foorginezhad, M. M. Zerafat, Y. Mohammadi, and M. Asadnia, "Fabrication of Tubular Ceramic Membranes as Low-Cost Adsorbent Using Natural Clay for Heavy Metals Removal," *Cleaner Engineering and Technology* 10 (2022): 100550, https://doi.org/10.1016/j.clet.2022.100550.

51. M. R. Adam, N. M. Salleh, M. H. D. Othman, et al., "The Adsorptive Removal of Chromium (VI) in Aqueous Solution by Novel Natural Zeolite Based Hollow Fibre Ceramic Membrane," *Journal of Environmental Management* 224 (2018): 252–262, https://doi.org/10.1016/j.jenvman.2018.07.043.

52. A. Majouli, S. A. Younssi, S. Tahiri, A. Albizane, H. Loukili, and M. Belhaj, "Characterization of Flat Membrane Support Elaborated From Local Moroccan Perlite," *Desalination* 277 (2011): 61–66, 10.1016/j.desal.2011.04.003.

53. K. Suresh, G. Pugazhenthi, and R. Uppaluri, "Fly Ash Based Ceramic Microfiltration Membranes for Oil-Water Emulsion Treatment: Parametric Optimization Using Response Surface Methodology," *Journal of Water Process Engineering* 13 (2016): 27–43, https://doi.org/10.1016/j.jwpe.2016.07.008.

54. S. K. Hubadillah, M. H. D. Othman, A. Ismail, et al., "Fabrication of Low Cost, Green Silica Based Ceramic Hollow Fibre Membrane Prepared From Waste Rice Husk for Water Filtration Application," *Ceramics International* 44 (2018): 10498–10509, https://doi.org/10.1016/j.ceramint.2018.03.067.

55. S. Sisnayati, R. Komala, and R. Suryani, "The Effect of Rice Husk Addition as Additive Materials on the Characterization of Ceramic Membrane and Their Application on Water River Treatment Process," *Science and Technology Indonesia* 4 (2019): 11–17, 10.26554/sti.2019.4.1.11-.

56. N. H. Kamarudin, Z. Harun, M. H. D. Othman, et al., "Waste Environmental Sources of Metakaolin and Corn Cob Ash for Preparation and Characterisation of Green Ceramic Hollow Fibre Membrane (h-MCa) for Oil-Water Separation," *Ceramics International* 46 (2020): 1512–1525, https://doi.org/10.1016/j.ceramint.2019.09.118.

57. K. Prabhakaran, A. Melkeri, N. Gokhale, and S. Sharma, "Preparation of *Macroporous alumina* Ceramics Using Wheat Particles as Gelling and Pore Forming Agent," *Ceramics International* 33 (2007): 77–81, https://doi.org/10.1016/j.ceramint.2005.07.020.

58. S. K. Hubadillah, M. H. D. Othman, Z. S. Tai, et al., "Novel Hydroxyapatite-Based Bio-Ceramic Hollow Fiber Membrane Derived From Waste Cow Bone for Textile Wastewater Treatment," *Chemical Engineering Journal* 379 (2020): 122396, https://doi.org/10.1016/j.cej.2019.122396.

59. Z. Zhong, D. Li, B. Zhang, and W. Xing, "Membrane Surface Roughness Characterization and Its Influence on Ultrafine Particle Adhesion," *Separation and Purification Technology* 90 (2012): 40–146, https://doi.org/10.1016/j.seppur.2011.09.016.

60. M. Boutaleb, K. Tabit, M. Mansori, L. Saâdi, and M. Waqif, "Development of Low-Cost Clayey Ceramic Filtering Membrane With Controllable

Porosity and High Mechanical Strength," *Ceramics International* 50, no. 18 (2024): 32771–32782, https://doi.org/10.1016/j.ceramint.2024.06.087.

61. F. Aouay, A. Deratani, A. Attia, L. Dammak, and R. B. Amar, "Bifunctional Ceramic Membranes From Spent Coffee Grounds for Selective Removal of Pharmaceuticals and Textile Dyes," *Separation and Purification Technology* 396, no. 2 (2026): 137971, 10.1016/j.seppur.2026.137971.

62. A. A. Alhwaige, H. Ishida, and S. Qutubuddin, "Poly(benzoxazine-f-chitosan) Films: The Role of Aldehyde Neighboring Groups on Chemical Interaction of Benzoxazine Precursors With Chitosan," *Carbohydrate Polymers* 209 (2019): 122–129, https://doi.org/10.1016/j.carbpol.2019.01.016.

63. M. L. L ópez Zavala, H. Romero-Santana, and B. Monárrez-Cordero, "Removal of Cr(VI) From Water by Adsorption Using Low Cost Clay-Perlite-Iron Membranes," *Journal of Water Process Engineering* 38 (2020): 101672, https://doi.org/10.1016/j.jwpe.2020.101672.

64. R. Campbell, B. Xiao, and C. Mangwandi, "Production of Activated Carbon From Spent Coffee Grounds (SCG) for Removal of Hexavalent Chromium From Synthetic Wastewater Solutions," *Journal of Environmental Management* 366 (2024): 121682, https://doi.org/10.1016/j.jenvman.2024.121682.

65. Q. Ren, X. Chen, Y. Yumminaga, et al., "Effect of Operating Conditions on the Performance of Multichannel Ceramic Ultrafiltration Membranes for Cattle Wastewater Treatment," *Journal of Water Process Engineering* 41 (2021): 102102, https://doi.org/10.1016/j.jwpe.2021.102102.

66. W. Aloulou, H. Aloulou, A. Attia, S. Chakraborty, and R. B. Amar, "Treatment of Tuna Cooking Juice via Ceramic Ultrafiltration Membrane: Optimization Using Response Surface Methodology," *Membranes* 12 (2022): 813, https://doi.org/10.3390/membranes12080813.

67. H. Aloulou, A. Attia, W. Aloulou, et al., "Statistical Simulation, a Tool for the Process Optimization of Oily Wastewater by Cross-flow Ultrafiltration," *Membranes* 12 (2022): 676, https://doi.org/10.3390/membranes12070676.

68. A. Abdullayev, M. F. Bekheet, D. A. H. Hanaor, and A. Gurlo, "Materials and Applications for Low-Cost Ceramic Membranes," *Membranes* 9, no. 9 (2019): 105, https://doi.org/10.3390/membranes9090105.

69. J. Bahrouni, H. Aloulou, A. Attia, L. Dammak, and R. B. Amar, "Surface Modification of a Zeolite Microfiltration Membrane: Characterization and Application to the Treatment of Colored and Oily Wastewaters," *Chemistry Africa* 7 (2024): 4513–4527, https://doi.org/10.1007/s42250-024-01035-9.

70. V. Bisht and C. Das, "Fabrication and Characterization of the Novel Tubular Ceramic Membrane Using Walnut Shells and Its Application in TiO_2 Nanoparticles Separation From Suspension," *Ceramics International* 50, no. 6 (2024): 8706–8717, https://doi.org/10.1016/j.ceramint.2023.12.187.